



Statistical Structure at the Wall of the High Reynolds Number Turbulent Boundary Layer

J.C.R. HUNT¹ and P. CARLOTTI²

¹*Departments of Space Climate Physics and Geological Sciences, University College, London WCI, U.K.; and J.M. Burgers Centre, Delft University of Technology, Delft, The Netherlands;*

²*Department of Applied Mathematics and Theoretical Physics, University of Cambridge, Cambridge, U.K.; and Centre National de Recherches Météorologiques, Météo France, Toulouse, France*

Received 19 April 2000; accepted in revised form 8 January 2001

Abstract. The one and two-point statistical structure of very high Reynolds number turbulence in the surface layer near a rigid ‘wall’ is analysed. The essential mechanisms for turbulent eddies impinging on the wall are studied using linearised rapid distortion theory, which show how the mean shear and blocking actions of the surface act first independently and then, over the life time of the eddy, interactively. Previous analytical results are reinterpreted and some new results are derived to show how the integral length scales, cross correlations and spectra of the different components of the turbulence are distorted depending on the form of the spectra of eddies above the surface layer and how they are related to motions of characteristic eddy structures near the surface. These results are applied to derive some quantitative and qualitative predictions in the surface layers (SL), where the eddies are affected by local shear dynamics, and in the ‘eddy surface layer’ (ESL) where quasi independent sloping elongated eddies interact directly with the wall, and where there is a large range of wavenumber within which the spectra of the horizontal velocity components are proportional to k^{-1} . The longest eddies in the boundary layer occur near the wall. Field experiments agree with the theoretical model predictions for the quite different forms for the spectra, cospectra and cross correlations for the vertical and horizontal components of the velocity field. By showing that in SL the energy exchange between the large and small scale eddies is local (‘staircase’) energy cascade, whereas in ESL there is a direct nonlocal (‘elevator-like’) energy transfer to the small scales, it is shown why the thickness of the ESL increases over rougher surfaces and as the Reynolds number decreases.

Key words: energy transfer, RDT, spectra, surface layer.

1. Introduction

Well established theories for the mean velocity and variances in turbulent flows close to a solid boundary are based on simple concepts about how the eddies scale and on the assumption that turbulence is in a state of local equilibrium (cf. [44, §5.4]). Further information and theory is needed to describe the eddy structure, estimate and explain the forms of the two-point statistics, and design a subgrid model for high Reynolds number Large Eddy simulation (LES) (cf. [40]). The new

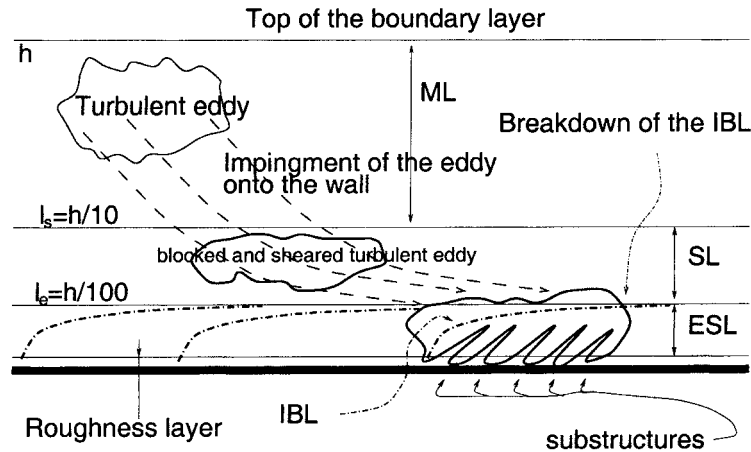


Figure 1. Sketch of a typical high Reynolds number boundary layer; $h \approx 1-2$ km, $l_s \approx 100-200$ m, $l_e \approx 10-20$ m, the roughness length z_0 is less than 0.1 m over a field, less than 1 m over a typical city.

concepts and data needed for this aspect of turbulence structure may be quite more sensitive to the Reynolds number than the equilibrium layer theory.

The aim of this paper is to use approximate theoretical models (e.g. [26, 31]) for distorted turbulent flows to calculate surface spectra and two-point correlations close to the wall for different forms of the spectra above the surface layer.

It has been shown by Hunt and Morrison [22] that the primary mechanism of eddy motion in low Reynolds number wall layers ($Re_\tau \lesssim 10^4$, based on the boundary layer thickness and the friction velocity) is 'bottom-up', whereas at very high Reynolds, there is evidence that turbulent boundary layers have more a 'top-down' behaviour (see Figure 1) As the eddies impinge, they are 'blocked' (B) by the wall, the vertical velocity being forced to tend to zero. But they also generate internal boundary layers (IBL) within each eddy because there is a boundary condition at the wall of zero tangential velocity. As the blocked vortices interact with each other near the surface, they burst upwards [11] causing 'anti-splats' [38] on the time scale of the outer structure. These differ from bursts in low Reynolds number boundary layers, which are driven by local instabilities on time scales of the order of ν/u_*^2 , i.e. orders of magnitude smaller than that of the outer structure bursts. This allows us to distinguish between the two types of bursts in experiments.

The blocking hypothesis has been partially verified experimentally by measuring whether the effects on the vertical component of turbulence are consistent with it, eg whether the variance $\overline{w^2}$ increases with height in the surface layer (see Section 3.1.1 and also [10]) and on two-point vertical correlations [21]. Another important experimental fact is the existence of elongated structures that have been inferred from several sets of spectral measurements (e.g. [8] or [25]) showing a very long k_1^{-1} self similar range in the streamwise spectrum (see Figure 2). These

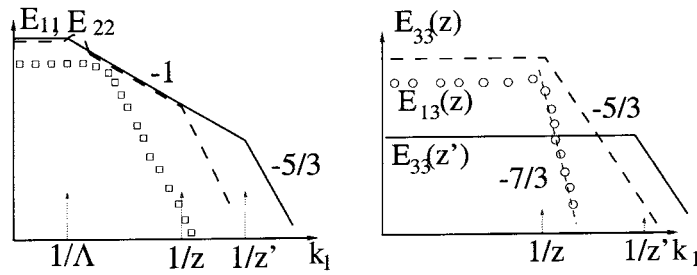


Figure 2. Measured spectrum in atmosphere and pipe; \square : spectra in the surface layer; solid and dashed lines: E_{11} , E_{22} and E_{33} in the eddy surface layer; \circ : E_{13} in the eddy surface layer.

very long structures, which are observed to be associated with surface shear (SS), have substructures consisting of sheared eddies on a range of length scales [1].

A high Reynolds number neutral boundary layer can be divided into three sub-layers where the *blocking* (B), *shear* (S), and *surface shear* (SS) mechanisms near the wall act on the turbulence in different ways (see Figure 1). In the middle layer (ML) the effects of shear and diffusion of turbulent energy dominate [44] (and the Coriolis forces in the case of the ideal atmospheric boundary layer), whereas in the surface layer (SL) both effects of shear and blocking are significant. From the experimental evidence presented above, we conclude that it is necessary to define an even thinner layer that we call the *eddy surface layer* (ESL) where the main effects are blocking (B) and the creation of internal boundary layers (IBL) in the eddies (SS) [1]. This layer is most clearly identified as the layer where the k^{-1} self similar range is observed for horizontal velocity fluctuations. If we denote by h the thickness of the boundary layer, that of the surface layer (ℓ_s) is typically $h/10$. In our new terminology, the eddy surface layer thickness ℓ_e is even smaller, being about $h/100$ in the atmospheric boundary layer. As we shall show, the usual description does not distinguish between surface layer and eddy surface layers; the latter needs a high enough Reynolds number to exist. Experimentally, the logarithmic mean velocity profile is observed in both SL and ESL; but experiments show that two-point quantities are very different in the two layers (Figure 2). Note that in laboratory experiments [25, 39], the ESL is thicker when scaled with h and may occupy all the SL ($\ell_e \approx h/3$). In the following, we concentrate on the atmospheric case, using results of laboratory experiments only for comparison. It is important to remember that the only imposed length scale for the atmospheric boundary layer is the roughness length z_0 , because the viscous scaling $z_* = \nu/u_*$ is much smaller. Typical values of the length scales are $h \approx 1$ km, $z_* \approx 0.02$ cm and $z_0 \approx 1$ to 10 cm in the countryside, up to a few meters above city centres. Therefore, $z_* \ll z_0 \ll h/100$ with a good accuracy.

In the SL, it has been shown (cf. [31]) that for a wavelength k then if $k < x_3^{-1}$, the main physical effect is the blocking of the large scales, and if $k > x_3^{-1}$ the main physical effect is the shearing and self straining of the turbulence. In the ESL, there have so far been few studies of the physical processes taking place. It

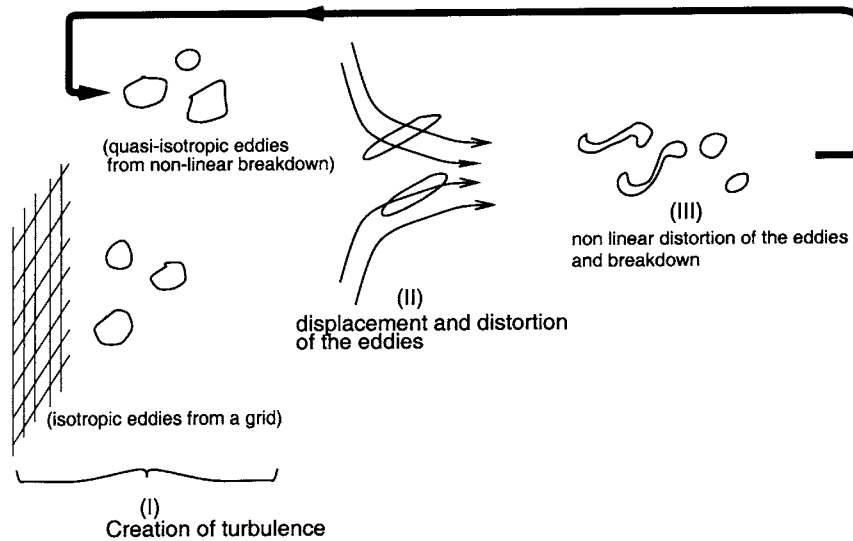


Figure 3. Principle of Rapid Distortion: the turbulence created in (I) is distorted in (II) on a fast time scale, and then decays in (III); (I) depends crucially on nonlinear effects, whereas (II) is mainly determined by linear distortion of the pre-existing eddies.

is proposed that the main mechanism is the formation of substructures in which there is a *direct* energy transfer to much smaller scales (where it is dissipated) as opposed to a progressive energy transfer to smaller scale of comparable magnitude by a step by step (or 'staircase') cascade.

In Section 2, we first develop some idealised mathematical models for the shear blocking mechanism. One consequence of this analysis is that the commonly assumed form of subgrid models for LES is not consistent with the traditional derivation of the log law of the wall using scaling analysis. Then in Section 3 we use these idealised models plus some heuristic arguments to propose a general formulation for the spectra consistent with experiments. Finally, in Section 4 we summarise the new concepts introduced here and point to future developments.

2. Idealised Shear-Blocking Models

We analyse here the effects of the three basic mechanisms (shear, blocking, and the combination of the two) on the turbulent eddies using linearised Rapid Distortion Theory (RDT) together with the assumption of a relaxation time which depends on the size of the eddies, $\tau(k)$ (cf. Figure 3), see [44]. First quasi isotropic turbulence is assumed (which might be generated by a grid or by the breakdown of previously distorted eddies); then it is advected and distorted by the mean flow on a time scale short enough that the dominant dynamics is linear. Later nonlinear distortion and eddy breakdown occur. In a steady state, all three stages are taking place simultan-

eously, but in many shear flows the second stage, where RDT is valid, determines the essential eddy structure.

In Section 2.1 we consider both linear RDT for an homogeneous shear, as initiated by Moffatt [35], and the nonlinear effects. Then, we consider shear free blocked turbulence using the inhomogeneous method of Hunt [14] (Section 2.2). The case of uniform shear and blocking is finally considered (Section 2.3). The main goal of these calculations is to show how the integral length scales and spectra of the different velocity components vary with distance x_3 from the surface and with the form of the spectrum above the surface, and the relative influences of shear and blocking on turbulence near a rigid surface.

2.1. UNIFORM SHEAR

In the ‘classical’ RDT calculation, an initially ($t = 0$) homogeneous and isotropic turbulent field in the whole space is distorted by an imposed mean shear for $t > 0$. We write the mean and fluctuating velocity fields as \underline{U} and \underline{u} ; in a uniform shear S , $\underline{U} = S \times x_3 \underline{e}_1$, where $(\underline{e}_1, \underline{e}_2, \underline{e}_3)$ is a vectorial basis (streamwise, spanwise and vertical directions); we use also the notation $\beta = St$ for the nondimensional shear. The Navier–Stokes equations for \underline{u} are:

$$\begin{cases} \partial_t u_i + U_j \partial_{x_j} u_i + u_j \partial_{x_j} U_i = -\partial_{x_i} p + (\text{NL})_i, \\ \partial_{x_i} u_i = 0, \end{cases} \quad (1)$$

$$\underline{u}(t = 0) = \underline{u}_0 \text{ homogeneous turbulent field,} \quad (2)$$

where $(\text{NL})_i = -\partial_j(u_i u_j)$ are the nonlinear terms. In the linearised form (RDT) of the equation these nonlinear terms are neglected. Because of the linearity of the RDT equations, to calculate the moments of order n , initial conditions are needed at this order (or less) only. Hence the initial spectral tensor Φ_{ij} and the mean velocity U_i are the only initial conditions needed to solve the problem of finding an analytical expression of Φ_{ij} as a function of time (see [17] and [31] for explicit results).

For high Reynolds number turbulence (i.e. turbulence with a Kolmogorov spectrum, $E(k) \sim \varepsilon^{2/3} k^{-5/3}$), the largest self induced strain is produced at small scales, where eddies with wavenumber k have strain rate s of order $s(k) = \varepsilon^{1/3} k^{2/3}$. So if the mean strain S is greater than that of the large eddies (with scale L^H), i.e. $s(1/L^H) < S$, there exist a critical wavenumber k^* where the mean and turbulent strain are of the same order, i.e. $S = s(k^*)$, whence $k^* \approx \varepsilon^{1/2} S^{3/2}$. For eddies larger than $1/k^*$, the amplified components of the linear solution is relevant. Note that $s(1/L^H) \sim u_0/L^H \sim 1/T_L$, where u_0 is the RMS velocity and T_L the Lagrangian time scale; thence k^* exists provided $S > u_0/L^H$ (cf. [17]).

Certain features (the ones concerning horizontal velocity components) of the linear solution remain valid for longer times (i.e. $\beta = St \gtrsim 1$) than other features

(or components). This occurs when the solution for the distorted feature or component is amplified or when the distorted solution reaches a constant form (as we see with blocking or streak structures) or when nonlinear amplification is reduced by linear distortion (cf. [23]). Thus, for $\overline{u_1^2}$, $\overline{u_2^2}$, and $\overline{u_1 u_3}$, the approximate linear calculation is valid provided β depends on the component to which it is applied. The value of β has to be determined by experiment or nonlinear calculation. For example, Townsend [44] used $\beta \approx 5$ for the calculation of τ/q^2 . However, in calculations of the variance $\overline{u_3^2}$, the result of the linear solution is a decrease, but with the nonlinear effects of eddy distortion and eddy movement there is a net increase (cf. the direct numerical simulation of Kida and Tanaka [24]). This occurs even where $\beta \leq 1$ or $t \leq T_L$.

The linear calculations made by Hunt and Carruthers [17, §4.4] showed that in a shear flow, in transitional or low Reynolds number turbulence (where the initial velocity field is smooth enough that $E(k, t = 0) \propto k^{-2p_0}$ with $2p_0 > 2$), the spectrum for finite time changes significantly so that $E_{11} \approx E_{22} \propto k^{-2}$ and $E_{33} \propto k^{-4}$. This spectral form is associated with step-like variation of the velocity component between elongated streamwise ‘streaks’. At low wavenumber, $E_{11}(k_1 \rightarrow 0)$ continues to increase with time and the streaks become more elongated. Dynamically these ‘streaks’ result from a linear process which is only slightly modified by nonlinear effects, such as those which makes the streaks meander (cf. [27]). In very high Reynolds number turbulence where the initial spectrum of turbulence has more small scale energy (i.e. a slower roll-off with $2p_0 < 2$), the formation of streaks and elongated sloping streamwise vortices is unaffected; but the velocity gradient due to these structures are less sharp (or their spatial distribution is less singular) than those due to the small scale turbulence. Here, these large structures only influence the shape of the spectrum at low wavenumber.

In flows where the mean shear S varies with height, it is known that the integral scale of the normal velocity fluctuations is $L_M^H \sim u_0/S$. Since the mean shear S decreases towards the top of the middle layer (ML, see Figure 1), L_M^H increases (cf. [21]). These longer scale fluctuations do not significantly influence the turbulence in the lower layers because of blocking at the wall and ‘sheltering’ caused by the gradient in the mean shear (cf. [18, 29]).

2.2. BLOCKING EFFECTS

2.2.1. Method

The simplest case of RDT for inhomogeneous turbulence near a rigid surface [14, 19]) is a calculation of the shear-free distortion of an initially homogeneous turbulent field \underline{u}^H after the introduction of a wall boundary condition at $x_3 = 0$ at initial time (see Figure 4). Since the vorticity equation reduces to $\overline{D\omega}/Dt = 0$ when $S = 0$, the only effect of the wall is to add an irrotational field $\nabla\phi$ to the turbulent velocity. This is in good agreement with experiments. Although for sim-

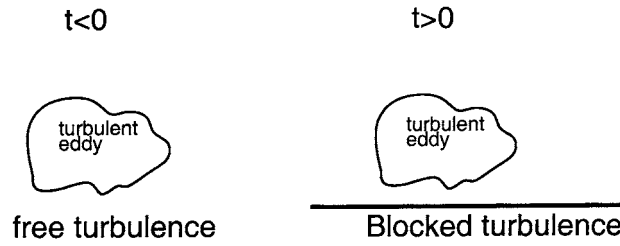


Figure 4. Introduction of a wall at $t = 0$ in the RDT blocking calculation.

plicity we assume here that for $t < 0$ the turbulence is homogeneous and isotropic, it can be shown that the effects of initial anisotropy are small [34].

Perot and Moin [38] noted in their appendix A that formally the incompressibility constraint does not hold between the times 0^- and 0^+ , because of the irrotational field $\nabla\phi$ added to the turbulent velocity by the presence of the wall. This is an elliptic, infinitely fast process (which guarantees a good accuracy of the theory), so that the linear calculations for statistical quantities do not depend on time for $t > 0$. (Recently Magnaudet [30] showed that this approximation is valid at any time for high Reynolds number boundary layer.) Hence for $t > 0$,

$$\begin{cases} \underline{u} = \underline{u}^H + \nabla\phi, \\ \partial_{x_3}\phi = -u_3^H \text{ at } x_3 = 0, \\ \nabla^2\phi = 0. \end{cases} \quad (3)$$

For the practical resolution of the problem two-dimensional Fourier transforms on horizontal planes can be used:

$$a_i(k_1, k_2, x_3) = \iint u_i(x_1, x_2, x_3)e^{i(k_1x_1+k_2x_2)} dx_1 dx_2. \quad (4)$$

The linearised Navier–Stokes equations lead to analytical expressions for amplitude and wavenumber variations as functions of initial conditions. As in the pure shear case, the only initial condition needed is the initial spectral correlation tensor. We assume that initially turbulence has a generalised von Karman-type spectrum of index $2p$,

$$E^H(k) = E_0 \frac{(kL^H)^4}{[1 + (kL^H)^2]^{2p+2}} \quad (5)$$

which matches the Kolmogorov inertial range spectrum at high wavenumbers for $2p = 5/3$ and agrees approximately with laboratory and atmospheric boundary layer data at small wavenumber (except in the eddy surface layer as shown in Section 3). The resulting inhomogeneous and anisotropic turbulence is described by a second order tensor. For the relevant components of Φ_{ij} :

$$\Phi_{11}(k_1, k_2, x_3) = \frac{1}{(2\pi)^2} \int \left[\Phi_{11}^H + k_1^2 \frac{e^{-2\kappa x_3}}{k^2} \Phi_{33}^H + \frac{2k_1}{\kappa} \sin k_3 x_3 e^{-\kappa x_3} \Phi_{13}^H \right] dk_3,$$

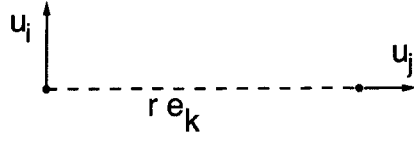


Figure 5. Definition of the integral scales.

$$\begin{aligned}\Phi_{22}(k_1, k_2, x_3) &= \frac{1}{(2\pi)^2} \int \left[\Phi_{22}^H + k_2^2 \frac{e^{-2\kappa x_3}}{\kappa^2} \Phi_{33}^H + \frac{2k_2}{\kappa} \sin k_3 x_3 e^{-\kappa x_3} \Phi_{23}^H \right] dk_3, \\ \Phi_{33}(k_1, k_2, x_3) &= \frac{1}{(2\pi)^2} \int \Phi_{33}^H \times |e^{-ik_3 x_3} - e^{-\kappa x_3}|^2 dk_3, \\ \Phi_{13}(k_1, k_2, x_3) &= \frac{1}{(2\pi)^2} \int \\ &\times \left[(1 - e^{-(\kappa + ik_3)x_3}) \Phi_{13}^H - i \frac{k_1}{\kappa} (e^{ik_3 x_3} - e^{-\kappa x_3}) e^{-\kappa x_3} \Phi_{33}^H \right] dk_3, \quad (6)\end{aligned}$$

where $\kappa = \sqrt{k_1^2 + k_2^2}$ and Φ_{ij}^H denote the homogeneous three-dimensional spectral correlation tensor valid for $t < 0$.

2.2.2. Inhomogeneous Length Scales of Turbulence

We define the integral scales $L_{ij}^{(x_k)\pm}$ for this inhomogeneous flow as functions of x_3 , viz.

$$L_{ij}^{(x_k)\pm}(x_3) = \frac{\int_0^X \overline{u_i(\underline{x}) u_j(\underline{x} \pm r \underline{e}_k)} dr}{R_{ij}(x_3, 0, 0, 0)}, \quad (7)$$

where $R_{ij}(r, \underline{x}) = \overline{u_i(\underline{x}) u_j(\underline{x} + r)}$ (see also Figure 5). The \pm is needed only for the case of the vertical length scales, meaning that the vertical integration runs above or below x_3 . $X = +\infty$ except for $L_{ij}^{(x_3)-}$, where $X = x_3$.

The RDT calculation gives analytic expressions of these integral scales in the form of ratios of integrals. These can be calculated analytically in the limit $x_3/L^H \rightarrow 0$ using the new systematic method developed by Carloti [2] for asymptotic expansions of integrals as functions of the spectrum roll-off (i.e. the exponent p). Taking a generalised von Karman spectrum of exponent $2p$, and nondimensionalising the length with L^H the integral of the initial homogeneous turbulence leads to the results shown in Table I. Note that in both cases, $\overline{u_3^2} \propto (x_3/L^H)^{2p-1}$.

This result is, at first sight, surprising, since the smoother the velocity field, (i.e. the less energy at the small scales), the larger the integral length scales near the surface, as shown in Figure 6. The physical reason is that close to the wall, when the small scales are filtered out from the integral, i.e. when the spectrum roll-off is fast, the scales that are affected by remote correlations are large (for

Table I. Asymptotic behaviour of integral scales.

$1 < 2p < 2$: slow roll off (typical of high Reynolds number turbulence)	$2 < 2p < 3$: fast roll off (typical of low Reynolds number turbulence or turbulence calculated with sub grid models)
$L_{33}^{(x_1)} \propto x_3$	$L_{33}^{(x_1)} \propto x_3^{3-2p}$
$L_{33}^{(x_2)} \propto x_3$	$L_{33}^{(x_2)} \propto x_3^{3-2p}$
$L_{33}^{(x_3)+} \propto x_3^{2-2p}$	$L_{33}^{(x_3)+} \propto x_3^{2-2p}$
$L_{33}^{(x_3)-} \propto x_3$	$L_{33}^{(x_3)-} \propto x_3$

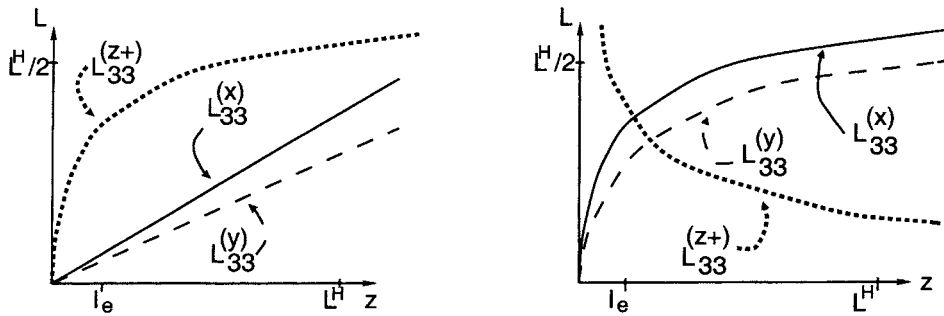


Figure 6. Integral scales in blocked turbulence; (a) $1 < 2p < 2$; (b) $2 < 2p < 3$.

further details, see [4]). There are three points to make about this result for turbulent length scales. First, for the high Reynolds number discussed in Sections 1 and 3, these results are indicative for the surface layer (SL) (see Figure 1). The analytical formulation breaks down in the eddy surface layer (ESL) because the spectrum does not have a von Karman form. The value of the length scale at $x_3 = \ell_e$ is therefore a ‘matching’ condition for the ESL. Second, an exponent $2p > 2$ can arise because of the subgrid model in a LES (which can be seen as a numerical simulation of moderate Reynolds number turbulence with high Reynolds number boundary conditions at the walls, cf. [33]). Third, Table I shows that if all the eddy scales are proportional to x_3 , then $2p \rightarrow 1$. As a corollary, if the spectral exponent $2p \neq 1$, the eddy length scales are not proportional to x_3 and therefore are inconsistent with the dimensional analysis formulation of the equilibrium log layer theory. This is another example of how scaling assumptions are not unique and that they are closely related to the form of spectra. The choice depends on identifying the appropriate mechanisms.

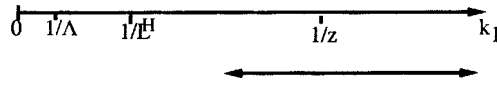


Figure 7. Range of validity of Equation (9).

2.2.3. Calculation of Spectra

In this region of strong shear, the surface frictional effects and the large mean shear near the ground stretch the vorticity of elongated eddies and produce a layered distribution of these eddies very close to the surface. This highly nonlinear process determines the form of the low wavenumber spectrum $E(k)$ when $k \lesssim x_3^{-1}$. Dimensional and statistical arguments [16, 39] show that $E(k)$ has a self-similar form

$$E(k) \sim k^{-2p} \tag{8}$$

with $2p = 1$ in the ESL. The approach taken here is to study the effect of blocking on different components for $k_1 < x_3^{-1}$ and $k_1 > x_3^{-1}$ by making the simplifying assumption that $E^H(k)$ has the same self similar form (8) over an *infinite* range.

Expressed in normalised form, the spectrum reads

$$E_{ij}(k_1, x_3) = \frac{1}{2\pi} \frac{E_0}{4\pi} k_1^{-2p} \tilde{\Phi}_{ij}(x'_3) \quad \text{with } x'_3 = k_1 x_3, \tag{9}$$

where the $E_{ij}(k_1, x_3) = \int \Phi_{ij}(k_1, k_2, x_3) dk_2$ and $\tilde{\Phi}_{ij}$ are unknown nondimensional functions. If the expression of the $\tilde{\Phi}_{ij}(x'_3)$ is given by RDT (blocking only), then:

$$\left\{ \begin{aligned} \tilde{\Phi}_{11}(x'_3) &= 4 \iint_{\mathcal{R}^{+2}} \frac{\xi^2 + \eta^2 + e^{-2\sqrt{1+\xi^2}x'_3} + \frac{-2\eta}{\sqrt{1+\xi^2}} e^{-\sqrt{1+\xi^2}x'_3} \sin \eta x'_3}{(1+\xi^2+\eta^2)^{2+p}} d\xi d\eta, \\ \tilde{\Phi}_{22}(x'_3) &= 4 \iint_{\mathcal{R}^{+2}} \frac{1+\eta^2+\xi^2 e^{-2\sqrt{1+\xi^2}x'_3} + \frac{-2\xi}{\sqrt{1+\xi^2}} e^{-\sqrt{1+\xi^2}x'_3} \sin \eta x'_3}{(1+\xi^2+\eta^2)^{2+p}} d\xi d\eta, \\ \tilde{\Phi}_{33}(x'_3) &= 4 \iint_{\mathcal{R}^{+2}} \frac{(1+\xi^2)|e^{-i\eta x'_3} - e^{-\sqrt{1+\xi^2}x'_3}|^2}{(1+\xi^2+\eta^2)^{2+p}} d\xi d\eta. \end{aligned} \right. \tag{10}$$

Note that $\tilde{\Phi}_{13} = 0$ as we can expect from symmetry considerations (cf. also below in this section). Further asymptotic régimes occur for $k_1 \ll 1/x_3$ and for $k_1 \gg 1/x_3$. The essence of this analysis is given in Figure 7, where the different relevant scales are compared. The case $k_1 \gg 1/x_3$ corresponds to very small structures, which do not feel the presence of the wall, whereas in the case $k_1 \ll 1/x_3$ the eddies are blocked; they are so anisotropic that they are almost two dimensional.

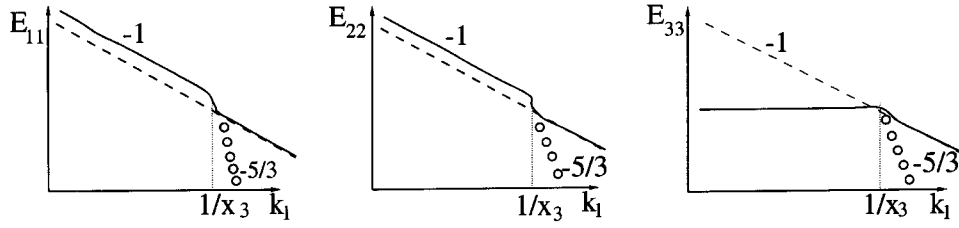


Figure 8. Distortion of spectra caused by blocking (calculated with RDT), assuming that the energy spectrum has a k^{-1} range. Dashed line (---): case of homogeneous turbulence; solid line (—): blocked turbulence; circles (o o o): observed spectrum for $k_1 > 1/x_3$.

Nondimensional spectra are given in Table II and their dimensional counterparts are:

$$\begin{array}{cc}
 \text{for } k_1 \ll 1/x_3 & \text{for } k_1 \gg 1/x_3 \\
 \left\{ \begin{array}{l} E_{11}(k_1, x_3) \sim \frac{1}{2p} \frac{E_0}{4\pi} k_1^{-2p}, \\ E_{22}(k_1, x_3) \sim \frac{1}{2p} \frac{E_0}{4\pi} k_1^{-2p}, \\ E_{33}(k_1, x_3) \sim \frac{A}{2\pi} \frac{E_0}{4\pi} x_3^{2p}, \end{array} \right. & \left\{ \begin{array}{l} E_{11}(k_1, x_3) \sim \frac{1}{2p(2p+2)} \frac{E_0}{2\pi} k_1^{-2p}, \\ E_{22}(k_1, x_3) \sim \frac{1+2p}{2p(2p+2)} \frac{E_0}{4\pi} k_1^{-2p}, \\ E_{33}(k_1, x_3) \sim \frac{1+2p}{2p(2p+2)} \frac{E_0}{4\pi} k_1^{-2p}. \end{array} \right. \quad (11)
 \end{array}$$

For $k_1 \ll 1/x_3$, the spectrum for the normal component is proportional to x_3^{2p} , but is constant with k_1 , while the tangential components have the same form as in the homogeneous unbounded turbulence, though it is increased by a factor $p + 1$ and $(2p+2)/(2p+1)$ respectively. The greater the spectral slope (or the less the relative energy of the small scales) the more rapidly does $E_{33}(k_1 \ll x_3^{-1})$ increase with x_3 and the greater the amplification of each wavenumber of the tangential component. Note that $E_{13} (= \Re(\hat{u}_1 \hat{u}_3))$ must by symmetry remain equal to zero. Therefore the Reynolds stresses remain equal to zero in the pure blocking case. The results are sketched in Figure 8 for the case $2p = 1$. For even larger scale motion near the wall, where $k_1 \ll (L^H)^{-1}$ the new spectra of the normal component are as given by Hunt and Graham [19]. The tangential components tend to the limits given by $E_{11}(k_1 L^H \rightarrow 0, z/L^H \rightarrow 0) \rightarrow E_{11}^H(k_1 = 0)$ and $E_{22}(k_1 L^H \rightarrow 0, z/L^H \rightarrow 0) \rightarrow \alpha E_{11}^H(k_1 = 0)$ where α is a numerical factor of order one.

2.3. SHEARED AND BLOCKED TURBULENCE

2.3.1. General Case

We review briefly here RDT calculations when both blocking and shear effects are taken into account, especially when the wavenumber is small. We follow Lee and Hunt [26] in assuming that the mean shear is uniform above a rigid ‘wall’ at $x_3 = 0$. The result can be expressed simply as

$$\underline{u} = \underline{u}^S + \underline{\nabla} \phi^B + \underline{u}^{SB}, \quad (12)$$

where \underline{u}^S is the homogeneous shear solution, $\underline{\nabla}\phi^B$ is the irrotational blocking solution (so that $\partial_{x_3}\phi = -u_3^S$ at $x_3 = 0$) and \underline{u}^{SB} is the extra term associated with the distortion of vorticity.

In a uniform shear boundary layer the RDT equation for the vorticity is

$$\frac{\overline{D\omega}}{Dt} = (\underline{\omega}\cdot\underline{\nabla})\underline{U} + (\underline{\Omega}\cdot\underline{\nabla})\underline{u}. \quad (13)$$

In a shear free boundary layer, $\nabla U = 0$ and $\Omega = 0$, and this equation reduces to $\overline{D\omega}/Dt = 0$, which is the reason for Equation (3), where the vorticity of the initial field is not modified. In a sheared boundary layer with blocking, because of the term $(\underline{\Omega}\cdot\underline{\nabla})\underline{u}$, where $\underline{\Omega} = \Omega e_2$, the fluctuating vorticity is changed. Because u_3 is reduced at the wall there is a reduction in $\overline{u_1^2}$ and $\overline{-u_1 u_3}$. For typical values of $\beta \sim 1$, the main effect of blocking (compared with the pure shear case, Section 2.1) is to reduce the normal velocity and increase the horizontal components. A complete quantitative result requires numerical evaluation of integrals (cf. [31]), but asymptotic limits can be derived analytically.

2.3.2. Case of a Small Streamwise Wavenumber

In this section, we consider the range of k_1 defined by $1/L^H \ll k_1 \ll 1/x_3$. To be able to use three-dimensional Fourier transforms, we extend all the fields for $x_3 < 0$, taking u and v even and w odd in order to fulfil automatically the boundary conditions. Writing the inviscid RDT equations with these hypotheses, one can see that the pressure term is negligible, as well as the term $Sx_3\partial_{x_1}w$. Therefore, in Fourier space,

$$\begin{cases} \partial_t \hat{w} \approx 0, \\ \partial_t \hat{u} \approx -S\hat{w}, \\ \hat{p} \approx 0, \end{cases} \quad (14)$$

and therefore

$$\begin{aligned} \hat{w} &\approx \hat{w}(t = 0^+), \\ \hat{u} &\approx \hat{u}(t = 0^+) - \beta \hat{w}(t = 0^+) \end{aligned} \quad (15)$$

for any time $\beta = St$.

This analysis is the same as for the low wavenumber limit of the uniform shear problem because the symmetries of Equation (14) are compatible with wall blocking boundary conditions, although this is not true for the full inviscid RDT equations. As in homogeneous shear, the value of β for which the linear theory is a good approximation differs for the various components of E_{ij} and must be found by comparison with experiments and heuristic arguments. We denote this by

β_{ij} . Thus if we denote E_{ij}^B as the spectra for the pure blocking case, since in the linearised frame work $E_{ij}(k_1, t = 0^+) = E_{ij}^B(k_1)$ and also $E_{13}^B = 0$, one gets

$$\begin{cases} E_{11}(k_1 \rightarrow 0, t) \sim E_{11}^B(k_1 \rightarrow 0) + \beta_{11}^2 E_{33}^B(k_1 \rightarrow 0), \\ E_{33}(k_1 \rightarrow 0, t) \sim E_{33}^B(k_1 \rightarrow 0), \\ E_{13}(k_1 \rightarrow 0, t) \sim -\beta_{13} E_{33}^B(k_1 \rightarrow 0). \end{cases} \quad (16)$$

The value of β_{13} for which the linear theory is valid is less than β_{11} , because E_{13} and E_{33} are dominated by smaller scales and because blocking is predominant for vertical components; typically, $\beta_{13} \approx 1$.

This method of applying first blocking and then shear gives a correct prediction for the Reynolds stress cospectrum $E_{13}(k_1 \rightarrow 0, t > 0)$ which could not, as explained in Section 2.2.3, be calculated by blocking alone. In other words, the result (16) shows that for low wavenumbers the distortion of the spectral components by shear is not changed by blocking. But because the normal stress or diagonal terms (E_{11} , E_{22} and E_{33}) are strongly affected by blocking, the relations between the components of E_{ij} are not the same in boundary layers as in uniform shear flows. Note that the analysis for the case of shear plus blocking is simplified because the mechanisms near the wall operate on different time scales, the shortest (instantaneous) being blocking, the next shear (z/u_*) and finally nonlinearity of the Navier–Stokes equation ($1/(u_*k)$).

3. Turbulence Structure and Two-Point Statistics in the Surface Layers

3.1. SURFACE LAYER

3.1.1. Variance of the Vertical Velocity

We now show how results of the statistical models of idealised flows provide a framework for analysing the structure of the turbulence in the surface layer (SL) and the eddy surface layer (ESL), and for estimating turbulence statistics.

Following Townsend [44] and Mann [31], blocking affects those eddies whose wavenumber k_c is less than about x_3^{-1} , where

$$k_c \sim \frac{(\partial_{x_3} U_1)^{3/2}}{\varepsilon^{1/2}} \sim x_3^{-1}. \quad (17)$$

In the SL of high Reynolds number sheared boundary layers, it is found experimentally that the integral scale $L_{11}^{(x_3)} \approx x_3/2$, whereas in both shear-free and convective boundary layers $L_{11}^{(x_3)} \approx x_3$ (cf. [21]). This is because the mean shear changes the form of the spectrum and amplifies the eddies smaller than the scale k_c^{-1} , which effectively reduces the length scales (see Section 2) (this is the assumption of most one-point turbulence models which generally ignore the blocking effects, except for Durbin's [7] wall reflection model and Craft and Launder's [5] anisotropy correction).

In shear-free boundary layers, because of blocking, the normal velocity component u_3 tends to zero as $x_3 \rightarrow 0$. In sheared boundary layers, as we saw in Section 2.3, blocking cannot be neglected. The variance of this shear-free component of velocity field, denoted here by $\overline{u_3^2}^B(x_3)$, represents the turbulence generated above the surface layer (SL) and impinging onto the ground (top-down). On the other hand, in near equilibrium sheared boundary layers the mean shear (and therefore the nonlinear shear production) increases toward the wall. This leads (cf. [43]) to local small scale production of turbulence in the surface layer, whose contribution to the variance is a shear contribution $\overline{u_3^2}^S \approx \lambda_S u_*^2$ where λ_S is a constant ($\lambda_S = 1.7$ following Townsend [44]). Because of the difference of scales of the two types of motion u^B and u^S , as in boundary layers with strong thermal convection and surface shear (cf. [36]), the vertical turbulence within SL can be described as the addition of two largely independent, shear and blocking components, the latter being produced by larger eddies at the top of the SL and the former by local shear, i.e. for $x_3 \lesssim \ell_S$, $\overline{u_3^2}(x_3) \approx \overline{u_3^2}^B(x_3) + \overline{u_3^2}^S(x_3)$.

Applying the results of Table II and of Hunt and Carruthers [17] for the pure shear component,

$$\overline{u_3^2} \approx \lambda_S u_*^2 + \overline{u_3^2}(x_3 = \ell_S)(x_3/\ell_S)^{2/3}. \quad (18)$$

This theoretically derived equation is in agreement with the measurement of $\overline{u_3^2}(x_3)$ by Högström [10] in a neutral boundary layer for $x_3 < 15$ m, (though in that paper he compared his data with another function that he had determined empirically, his data can be replotted to match very closely Equation (18)). These experimental data were an important and, at that time, controversial finding, because it indicates that even in the neutrally stratified boundary layer the vertical turbulence increases with height in the lower part of SL. For the blocking contribution the reference height is taken as the top of the surface layer (SL) where $x_3 \approx \ell_S$, because above this height the variance decreases and the integral scale of the vertical fluctuations $L_{11}^{(x_3)}(x_3)$ is significantly less than the distance x_3 to the surface. Also the shear stress and therefore the contribution $\overline{u_3^2}^S$ decreases above this level. A similar formula as (18) determines the vertical fluctuations in the convective boundary layer for $x_3 \leq \ell_S$, see [15].

3.1.2. Spectra in the SL

In the surface layer, where $x_3 < \ell_S$, as in all very high Reynolds number turbulent flows, the two-point second moment spectra at the scales less than the integral scale L^H (and larger than the microscale) have the universal form of the Kolmogorov inertial range (i.e. $E(k) \propto \varepsilon^{2/3} k^{-5/3}$). Although the energy spectrum for the largest scales decreases as $k \rightarrow 0$, and approximates to the widely observed form of large scale homogeneous turbulence, i.e. $E(k) \propto k^4$, the spectra of the different large scale components differ from homogeneous, being affected by blocking and shear-

ing mechanisms, because $\ell_s \sim L^H(x_3 \sim \ell_s) \sim h/5$. It follows from Section 2 that the horizontal components approximately have the same form as in homogeneous shear, even where blocking effects are significant; so that at high Reynolds number,

$$\text{for } k_1 \gtrsim (L^H)^{-1}, \quad E_{11} \sim E_{22} \sim \varepsilon(x_3)^{2/3} k_1^{-5/3} \approx u_*^2 x_3^{-2/3} k_1^{-5/3}. \quad (19)$$

However from Table II, the normal component spectrum is

$$E_{33} \approx u_*^2 x_3^{-2/3} k_1^{-5/3} \quad \text{for } k_1 > x_3^{-1}, \quad (20a)$$

$$\approx u_*^2 x_3^{-2/3} x_3^{5/3} = u_*^2 x_3 \quad \text{for } k_1 < x_3^{-1}. \quad (20b)$$

Using the results of the linear theory of Section 2.3, it follows that the Reynolds stress cospectrum is also ‘flat’ at low wavenumber, i.e.:

$$E_{13} \sim \beta_{13} E_{33} \sim u_*^2 x_3 \quad \text{for } k_1 \ll x_3^{-1}. \quad (21)$$

The coefficient β_{13} is of order 1. For $k_1 > x_3^{-1}$, the turbulence is slightly anisotropic, so that the diagonal terms of the spectral tensor (E_{11} , E_{22} and E_{33}) differ slightly from each other and the nonsymmetric terms are nonzero. These deviations can be estimated using linear theory by calculating the net strain experienced by eddies distorted by the mean shear over the relaxation time $\tau(k)$ of eddies of size k^{-1} (following Mann [31]). Since $\tau(k) \sim \varepsilon^{-1/2} k^{-2/3}$, the cospectrum decreases rapidly with wavenumber (more rapidly than the spectra), viz

$$E_{13} \approx \varepsilon^{1/3} \partial_{x_3} U_1 k_1^{-7/3} \approx u_*^2 x_3^{-5/3} k_1^{-7/3} \quad (22)$$

(see [31]). All these equations match each other (in order of magnitude terms) when $k_1 \approx x_3^{-1}$. Integrating the spectrum E_{33} and the cospectrum E_{13} shows that for the locally produced shear turbulence, $\overline{u_3^2}$ and $-\overline{u_1 u_3}$ are constant with height in the SL. As shown in Equation (18) there is also a contribution from ‘inactive’ fluctuations produced by larger scale fluctuations in the upper part of SL.

3.1.3. Two Point Vertical Correlations

The effects of blocking were shown by Hunt [15] and Hunt et al. [21] to dominate the two-point correlation of the vertical component even in sheared boundary layers (at high Reynolds number). Following the same argument as in Section 3.1.1 of separation of u^S and u^B ,

$$\hat{R}_{33} = \frac{\overline{u_3(x_3)u_3(x'_3)}}{\overline{u_3^2(x_3)}} \approx \frac{\overline{(u_3^S(x_3) + u_3^B(x_3))(u_3^S(x'_3) + u_3^B(x'_3))}}{\overline{(u_3^S)^2 + (u_3^B)^2(x_3)}}. \quad (23)$$

The greatest contributions to the velocity cross correlation is generated by energetic eddies at different heights with approximately the same range of wavenumbers. Thus at a height x'_3 , the eddies that correlate with those at a lower level $x_3 < x'_3$

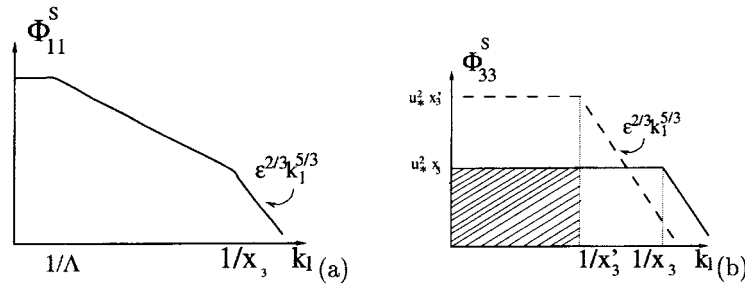


Figure 9. Spectra in ESL according to our theory.

are those which are larger than or of the same order as the height x_3 , i.e. $k_1 \leq x_3^{-1}$; thence it follows from the form of the spectra for the shear turbulence and blocking turbulence (shaded area in Figure 9) that the cross correlations of the different eddy components in Equation (23) are

$$\begin{aligned} \overline{u_3^S(x_3)u_3^S(x_3')} &\approx (x_3'/x_3)\overline{u_3^S(x_3)}, \\ \overline{u_3^B(x_3)u_3^B(x_3')} &\approx (x_3'/x_3)\overline{u_3^B(x_3)}. \end{aligned} \tag{24}$$

Since the ‘sheared’ and ‘blocked’ eddies are not strongly correlated, as explained in Equation (18), it follows from Equations (23) and 24 that for the surface layer,

$$\hat{R}_{33} \approx x_3'/x_3. \tag{25}$$

Of course this is an exact asymptotic result for pure blocking flows (where $u_3^S = 0$). Experimental measurements of \hat{R}_{33} for a range of x_3' and x_3 from 10 to 300 meters at the Boulder Atmospheric Observatory (cf. [21]) in sheared and convective flows are consistent with Equation (25). A more detailed discussion will be published in [3].

3.2. EDDY SURFACE LAYER (ESL)

3.2.1. Direct Transfer of Energy and Attached Eddies

In this layer very close to the surface the dynamics of the low wavenumber end of the spectrum is influenced by the surface through the creation of an internal boundary layer within each individual large eddy (IBL, see Figure 1), and by the shedding of vorticity from the highly deformed and relatively fast moving eddies as they descend into the slow moving air near the ground. Thus, in each eddy, of wavenumber $k_1 \lesssim x_3^{-1}$, there is a production of turbulent energy and, because of frictional dissipation caused by the wall and the diffusion of vorticity in this layer, there is a *direct*, or ‘elevator-like’, transfer towards smaller scales $k \gg x_3^{-1}$. Since these eddies only interact weakly with each other in this surface layer, this transfer process does not involve an eddy to eddy (or ‘staircase-like’) energy cascade (see

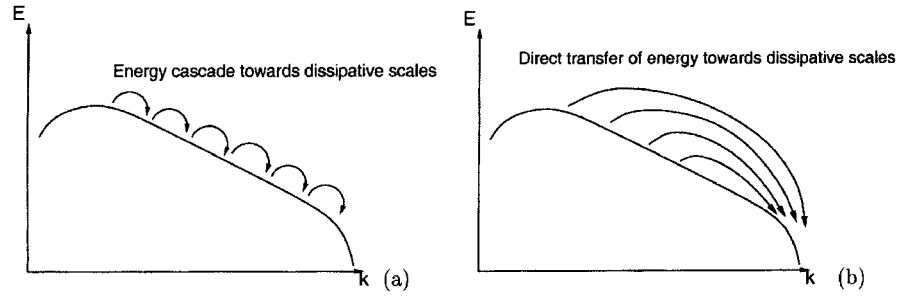


Figure 10. Schematic of the direct transfer phenomenon: (a) local interaction or ‘staircase’ cascade; (b) long range interaction or ‘elevator-like’ transfer of energy.

Table II. Nondimensional spectra: asymptotic expressions given by RDT.

$x'_3 \rightarrow 0$ i.e. $k_1 \ll 1/x_3$	$x'_3 \rightarrow \infty$ i.e. $k_1 \gg 1/x_3$
$\tilde{\Phi}_{11}(x'_3) \rightarrow \frac{2\pi}{2p}$	$\tilde{\Phi}_{11}(x'_3) \rightarrow \frac{4\pi}{2p(2p+2)}$
$\tilde{\Phi}_{22}(x'_3) \rightarrow \frac{2\pi}{2p}$	$\tilde{\Phi}_{22}(x'_3) \rightarrow \frac{2\pi(1+2p)}{2p(2p+2)}$
$\tilde{\Phi}_{33}(x'_3) \sim Ax_3^{2p}$ (for $2p = 1, A \approx 1.1$)	$\tilde{\Phi}_{33}(x'_3) \rightarrow \frac{2\pi(1+2p)}{2p(2p+2)}$

Figure 10). The scales of these weakly coupled large eddies extend over a range lying between x_3 (below which the inertia cascade determines the eddy dynamics), and Λ . The reason why Λ is significantly greater than the boundary layer depth is the shear straining and vorticity diffusion of the descending eddies. The observed self replication of surface ‘cat-paws’ that extend in long lines parallel to the wind (cf. [22]), which can be understood as the wake of the fast moving large eddies in the slow moving air near the ground, is a further reason why Λ should be large. It can be as large as 3000 m in the atmospheric boundary layer, and $18R$, where R is the pipe radius, in pipe flow experiments [25].

Summarising the results of the theory in the range $\Lambda^{-1} \ll k_1 \ll x_3^{-1}$,

$$E_{11}(k_1) \approx E_{11}(k_1, t = 0) = E_{11}^B(k_1) = c_{11}u_*^2k_1^{-1}, \tag{26a}$$

$$E_{22}(k_1) \approx E_{22}(k_1, t = 0) = E_{22}^B(k_1) = c_{22}u_*^2k_1^{-1}, \tag{26b}$$

$$E_{33}(k_1) \approx E_{33}(k_1, t = 0) = E_{33}^B(k_1) = c_{33}u_*^2x_3. \tag{26c}$$

The shear mainly determines the ratio of the constants c_{11} , c_{22} , and c_{33} . Blocking only gives the correct trend anyway, $c_{11}/c_{33} \approx 5.7$ and $c_{11}/c_{22} = 1$ (from Table II).

Table III. Comparison of present theory with experimental data; note that the data of [8] show a bump on the E_{33} spectrum at low wavenumber that may be caused by that fact that the measurements are made above the sea, where waves may form.

	mean shear (s^{-1})	c_{11}/c_{22}	c_{11}/c_{33}
RDT calculation	0	1	5.7
measurements Ref. [13]	0.7–1.6	2	4
measurements Ref. [8]	1.2	1.2	1.3

Typical values from experiments are shown in Table III. The mean shear crucially determines the Reynolds stress cospectrum, so that, using the results of Section 2.3,

$$E_{13}(k_1) \approx -\beta_{13} E_{33}^B(k_1) \sim -c_{33} u_*^2 x_3 \quad (27)$$

since $\beta_{13} \sim 1$. The results of Equations (20b), (21), (26c), (27) are new, but are consistent with the model of Townsend [44] modified by Perry et al. [39] of the near wall structure as constructed in term of ‘attached’ eddies.

3.2.2. Depth of the ESL

Given these results it is now possible to estimate heuristically the depth ℓ_e of the eddy surface layer. There the typical velocity in the large eddies is $u_1^{(e)}$ and these eddies develop internal boundary layers (IBL, cf. Figure 1). The velocity at height ℓ_e is denoted by u_e . In the internal boundary layer (IBL) of each eddy there is dissipation by eddy to eddy energy cascade $\varepsilon_{\text{cascade}}$ and also direct dissipation of energy by the internal shear ε_{ibl} as the eddies scrape along the surface. The total dissipation in the boundary layer, acting on the scale of the small isotropic eddies, is given by (where τ_e is the value of the surface stress for the eddy)

$$\varepsilon = (\tau + \tau_e) \partial_{x_3} (\bar{u} + u_1^{(e)}).$$

Summing its two components, $\varepsilon = \varepsilon_{\text{cascade}} + \varepsilon_{\text{ibl}}$. Here $\varepsilon_{\text{cascade}} = \tau \partial_{x_3} \bar{u}$ represents the eddy to eddy energy cascade, i.e. $\varepsilon_{\text{cascade}} = u_*^3 / (\kappa x_3)$, and

$$\varepsilon_{\text{ibl}} = \tau \partial_{x_3} u_1^{(e)} + \tau_e \partial_{x_3} \bar{u} + \tau_e \partial_{x_3} u_1^{(e)} \quad (28)$$

represents the direct transfer of energy from large scales to dissipative scales (caused by the internal boundary layer of each eddy). The dominant mechanism in the SL is the eddy to eddy cascade, and well above the ESL, $\langle \varepsilon_{\text{ibl}} \rangle \varepsilon_{\text{cascade}} \leq 1$. Therefore it is proposed here that the top of the ESL is the height ℓ_e below which the two processes of dissipation are on average of the same order (the average being taken on the large eddies):

$$\langle \varepsilon_{\text{ibl}} \rangle_{\text{eddies}} \sim \varepsilon_{\text{cascade}}. \quad (29)$$

By considering the means of the fluctuating quantities associated with the elongated surface layer eddies, it follows that in Equation (28), $\langle \tau \partial_{x_3} u_1^{(e)} \rangle_{\text{eddies}} = 0$ and $\langle \tau_e \partial_{x_3} \bar{u} \rangle_{\text{eddies}} = 0$ and therefore

$$\langle \varepsilon_{\text{ibl}} \rangle_{\text{eddies}} \approx \langle \tau_e \partial_{x_3} u_1^{(e)} \rangle_{\text{eddies}}. \quad (30)$$

At very high Reynolds number, in each eddy near the surface there is an ‘internal log law’ profile, so that (as in other perturbed turbulent boundary layer, e.g. [20]):

$$u_1^{(e)} \approx \frac{\sqrt{\tau_e}}{\kappa} \ln x_3/z_0. \quad (31)$$

Thence from Equation (30)

$$\langle \varepsilon_{\text{ibl}} \rangle_{\text{eddies}} \sim \kappa^2 \langle u_1^{(e)3} \rangle_{\text{eddies}} / [x_3 \ln^3(x_3/z_0)]. \quad (32)$$

Now, from integrating the spectrum (Equation (26)) for the large scales, where $x_3 \sim \ell_e$, $u_1^{(e)RMS} \approx u_* [1 + \ln \Lambda/x_3]^{1/2}$ (again, where $x_3 \ll \ell_e$, the value of $u_1^{(e)}$ decreases to zero in proportion to $\ln(x_3/z_0)$). The constant term comes from the very large eddies (of size larger than Λ) and the logarithmic term from the eddies of size between Λ and x_3 . It follows that the ESL height must satisfy the criterion

$$\kappa^2 u_*^3 [1 + \ln(\Lambda/\ell_e)]^{3/2} / [\ell_e \ln^3(\ell_e/z_0)] \sim u_*^3 / (\kappa \ell_e),$$

whence (ignoring constants of order one),

$$1 + \ln(\Lambda/\ell_e) \sim \ln^2 \ell_e/z_0 \quad (33)$$

to which the explicit solution is

$$\ell_e \approx z_0 \exp \left[\left(\sqrt{1 + 4(1 + \ln \Lambda/z_0)} - 1 \right) / 2 \right] \quad (34)$$

so that the thickness of the eddy surface layer increases with surface roughness. Thus when $z_0 \approx 10$ cm and $\Lambda \approx 3 \times 10^3$ m (as in the field experiments reviewed by Hunt and Morrison [22]), $\ell_e \approx 2$ m. This is consistent with the estimate of Hoxey and Richards [13] over agricultural fields and with the data plotted by Davenport [6] over suburban areas (where $z_0 \approx 0.3$ m and $\ell_e \approx 30$ m). Note that for typical laboratory flows over smooth surfaces where we can write $z_0 = 10\nu/u_*$, the boundary layer depth is $h \approx 10^3\nu/u_*$ and $\Lambda \approx 10^4\nu/u_*$, $\ell_e \approx h/5$; in other words, the eddy surface layer thickness (where a k^{-1} range is observed in the spectrum) is comparable with that of the surface layer. This is consistent with Marusic and Perry’s [32] measurements of boundary layers over smooth surfaces in this range of Reynolds numbers.

3.2.3. Reynolds Stresses and Log Layer

Certain statistics are the same in these two layers; in particular, the shear stress

$$\tau = \int_{-\infty}^{\infty} E_{13}(k_1) dk_1$$

is constant with height (from Equations (21) and (27)) and the dissipation length scale $L_\varepsilon = u_*^3/\varepsilon$ is of order x_3 . Thence following the analysis of Townsend [43] (or by noting how L_ε is affected by both the mean shear and blocking, cf. [21]), it appears that *the mean velocity profile has the same logarithmic form in both layers*

$$\overline{u_1} = \frac{u_*}{\kappa} \ln(x_3/z_0).$$

In the case, that we have not considered so far, of a flat (smooth) surface, a viscous sublayer (VSL) exists below the ESL (in place of the roughness layer). There the Reynolds number of the turbulent eddies decreases to zero at the wall. In the modelling of the upper part of VSL the turbulent structure is probably dominated by streaks driven by local shear and, as Lin et al. [28] have measured, the theoretically predicted k^{-2} spectra are observed at high wavenumber in the streamwise component (see Section 2).

4. Final Remarks

Hitherto unexplained high Reynolds number turbulent boundary layer measurements can be explained in terms of a dominant mechanism of ‘top-down’ eddies which are blocked and distorted by the strong surface shear, as they scrape along the surface. An application of rapid distortion theory with suitable physical hypotheses leads to a quantitative description of two-point statistics of the velocity field in the lower part of the surface layer. These models are complementary to the description of the upper part of the surface layer and middle layer by Mann [31]. We have also shown how, if the spectrum decays simply as a power law k^{-2p} , then (cf. Table I) the vertical length scale of the vertical component of turbulence varies as x_3^{2-2p} . When deriving the log law of the wall by dimensional analysis, one implicitly assumes that all the length scales vary proportionally to x_3 . Thence, as the theory demonstrates, all the eddies whose scales are larger than x_3 have an anisotropic structure and an energy spectrum that varies in proportion to k^{-1} . However, this result is not included in the subgrid models for LES near a wall, where it is generally assumed that the Kolmogorov $-5/3$ inertial range continues to be valid [42]. This is likely to explain the discrepancy between LES results and surface scaling arguments (cf. [40]). The new model presented here is consistent with the new approaches to near wall turbulence modelling in one-point models by Durbin [7] and Craft and Launder [5].

This study has shown how the energy transfer mechanisms are significantly changed by the large distortion of turbulence near the wall. These effects need

to be studied further, perhaps following the ideas proposed by Parpais [37] and reviewed by Godefert et al. [9].

Acknowledgements

It was an honour to present this paper at the symposium held in honour of Hieu Ha Minh, who was a distinguished research engineer and a great enthusiast for international collaboration in fluid mechanics. The work of JCRH was partly sponsored by Trinity College where he was a senior research fellow; PC is funded by the French Ministère de l'Équipement, des Transports et du Logement, where he is ingénieur des Ponts et Chaussées, through a mise à disposition de Météo France. We are grateful for many helpful ideas in preparing this paper from many colleagues, especially J.F. Morrison, U. Högström, the late A.E. Perry, J.J. Jimenez, F.T.M. Nieuwstadt, F. Hussain, and from anonymous referees.

References

1. Adrian, R.J. Meinhart, C.D. and Tomkins, C.D., Vortex organisation in the outer region of the turbulent boundary layer. *J. Fluid Mech.* **422** (2000) 1–54.
2. Carloti, P., General analysis of Fourier-type integrals with singular asymptotic expansions, in preparation.
3. Carloti, P., A study of two points properties of atmospheric turbulence using a high resolution LES. *Bound. Layer Meteor.* (2001) submitted.
4. Carloti, P., Distorted turbulence near rigid boundaries. Ph.D. Thesis, University of Cambridge (2001).
5. Craft, T.J. and Launder, B.E., A Reynolds stress closure designed for complex geometries. *Internat. J. Heat Fluid Flow* **17** (1996) 245–254.
6. Davenport, A.G., The spectra of horizontal gustiness near the ground in high winds. *Quart. J. Roy. Meteorol. Soc.* **LXXXVII** (1961) 194–211.
7. Durbin, P.A., A Reynolds stress model for near wall turbulence. *J. Fluid Mech.* **249** (1993) 465–498.
8. Fuehrer, P.L. and Friehe, C.A., A physically-based turbulent velocity time series decomposition. *Boundary Layer Meteorol.* **90**(2) (1999) 241–295.
9. Godefert, F., Cambon, C. and Scott, J., Report on the workshop ‘Two-point closures and their applications’. *J. Fluid Mech.* (2001) to appear.
10. Högström, U., Analysis of turbulence structure in the surface layer with a modified similarity formulation for near neutral conditions. *J. Atmospheric Sci.* **47**(16) (1990) 1949–1972.
11. Högström, U. and Bergström, H., Organised turbulence structures in the near-neutral atmospheric surface layer. *J. Atmospheric Sci.* **53**(17) (1996) 2452–2464.
12. Högström, U. Hunt, J.C.R. and Smedman, A.S., Theory and measurements for two points turbulence statistics in the high Reynolds number neutral surface layer, in preparation.
13. Hoxey, R.P. and Richards, P.J., Spectral characteristics of the atmospheric boundary layer near the ground. In: *1st UK Wind Engineering Conference*, Cambridge (1992).
14. Hunt, J.C.R., A theory of turbulent flow round two-dimensional bluff bodies. *J. Fluid Mech.* **61**(4) (1973) 625–706.
15. Hunt, J.C.R., Turbulence structure in thermal convection and shear-free boundary layers. *J. Fluid Mech.* **138** (1984) 161–184.

16. Hunt, J.C.R., Dynamics and statistics of vortical eddies in turbulence. In: Hunt, J.C.R. and Vassilicos, J.C. (eds), *Turbulence Structure and Vortex Dynamics*. Cambridge University Press, Cambridge (2001).
17. Hunt, J.C.R. and Carruthers, D.J., Rapid distortion theory and the 'problems' of turbulence. *J. Fluid Mech.* **212** (1990) 497–532.
18. Hunt, J.C.R. and Durbin, P.A., Perturbed vortical layers and shear sheltering. *Fluid Dynam. Res.* **24** (1999) 375–404.
19. Hunt, J.C.R. and Graham, J.M.R., Free-stream turbulence near plane boundaries. *J. Fluid Mech.* **84** (1978) 209–235.
20. Hunt, J.C.R., Leibovich, S. and Richards, K.J., Turbulent shear flows over hills. *Quart. J. Roy. Meteorol. Soc.* **114** (1988) 1435–1470.
21. Hunt, J.C.R., Moin, P., Lee, M., Moser, R.D., Spalart, P., Mansour, N.N., Kaimal, J.C. and Gaynor, E., Cross correlation and length scales in turbulent flows near surfaces, In: Fernholz, H.H. and Fiedler, H.E. (eds), *Advances in Turbulence*, Vol. 2. Springer-verlag, Berlin (1989) pp. 128–134.
22. Hunt, J.C.R. and Morrison, J.F., Eddy structure in turbulent boundary layers. *Eur. J. Mech. B – Fluids* **19** (2000) 673–694.
23. Kevlahan, N. and Hunt, J.C.R., Nonlinear interactions in turbulence with strong irrotational straining. *J. Fluid Mech.* **337** (1997) 333–364.
24. Kida, S. and Tanaka, M., Dynamics of vortical structures in homogeneous shear flows. *J. Fluid Mech.* **274** (1994) 43–68.
25. Kim, K.C. and Adrian, R.J., Very large-scale motion in the outer layer. *Phys. Fluids* **11**(2) (1999) 417–422.
26. Lee, M.J. and Hunt, J.C.R., The structure of sheared turbulence near a plane boundary. In: *Proceedings 7th Symposium on Turbulent Shear Flows*, Stanford, CA (1989) pp. 8.1.1–8.1.6.
27. Lee, M.J., Kim, J. and Moin, P., Structure of turbulence at high shear rate. *J. Fluid Mech.* **216** (1990) 561–583.
28. Lin, Z.C., Adrian, R.J. and Hanratty, T.J., A study of streaky structures in turbulent channel flow with particle image velocimetry. In: *Proceedings 8th International Symposium on Applied Laser Techniques to Fluid Mechanics*, Lisbon (1996).
29. Lumley, J.L., Yang, Z. and Shih, T.H., A length-scale equation. *Flow, Turbulence, Combustion* **63** (2000) 1–21.
30. Magnaudet, J., The structure of high Reynolds number turbulence close to a flat shear free surface. Part II. Validity and implications of rapid distortion theory predictions. *J. Fluid Mech.* (2000) submitted.
31. Mann, J., The spatial structure of neutral atmospheric surface layer turbulence. *J. Fluid Mech.* **273** (1994) 141–168.
32. Marusic, I. and Perry, A.E., A wall-wake model for turbulence structure of boundary layer – Part 2: Further experimental support. *J. Fluid Mech.* **298** (1995) 389–407.
33. Mason, P.A., Large eddy simulation: A critical review of the technique. *Quart. J. Roy. Meteor. Soc.* **120** (1994) 1–26.
34. Maxey, M.R., Distortion of turbulence in flows with parallel streamlines. *J. Fluid Mech.* **124** (1982) 261–282.
35. Moffatt, H.K., Interaction of turbulence with strong wind shear. In: Yaglom, A.M. and Tatarski, V.I. (eds), *Proceedings of the URSI-IUGG International Colloquium on Atmospheric Turbulence and Radio Wave Propagation*. Nauka, Moscow (1967) pp. 139–154.
36. Panofsky, H.A., Tennekes, H., Lenschow, D.H. and Wyngaard, J.C., The characteristics of turbulent velocity components in the surface layer under convective conditions. *Boundary Layer Meteorol.* **11** (1977) 355–361.
37. Parpais, S., Développement d'un modèle spectral pour la turbulence inhomogène; résolution par une méthode d'éléments finis. Ph.D. Thesis, Ecole Centrale de Lyon (1997).

38. Perot, B. and Moin, P., Shear free turbulent boundary layers. Part 1. Physical insight into near wall turbulence. *J. Fluid Mech.* **295** (1995) 199–227.
39. Perry, A.E., Henbest, S. and Chong, M.S., A theoretical and experimental study of wall turbulence. *J. Fluid Mech.* **165** (1986) 163–179.
40. Redelsperger, J.L., Mahé, F. and Carlotti, P., A simple and general approach enabling to sub-grid models to be suitable both for surface layer and free stream turbulence. *Boundary Layer Meteorol.* (2000) submitted.
41. Richards, P.J., Fong, S. and Hoxey, R.P., Anisotropic turbulence in the atmospheric surface layer. *J. Wind Engrg. Indust. Aerodynam.* **69–71** (1997) 903–913.
42. Schmidt, H. and Schumman, U., Coherent structure of the convective boundary layer derived from large eddy simulations. *J. Fluid Mech.* **200** (1989) 511–562.
43. Townsend, A.A., Equilibrium layers and wall turbulence. *J. Fluid Mech.* **11** (1961) 97–120.
44. Townsend, A.A., *The Structure of Turbulent Shear Flow*. Cambridge University Press, Cambridge (1976).